WPPFC-PR(18) 20163

M.J. Simmonds et al.

Isolating the Detrapping of Deuterium in Heavy Ion Damaged Tungsten via Partial Thermal Desorption

Preprint of Paper to be submitted for publication in
Journal of Nuclear Materials

This work has been carried out within the framework of the EUROfusion Consortium and has received funding from the Euratom research and training programme 2014-2018 under grant agreement No 633053. The views and opinions expressed herein do not necessarily reflect those of the European Commission.

This document is intended for publication in the open literature. It is made available on the clear understanding that it may not be further circulated and extracts or references may not be published prior to publication of the original when applicable, or without the consent of the Publications Officer, EUROfusion Programme Management Unit, Culham Science Centre, Abingdon, Oxon, OX14 3DB, UK or e-mail Publications.Officer@euro-fusion.org

Enquiries about Copyright and reproduction should be addressed to the Publications Officer, EUROfusion Programme Management Unit, Culham Science Centre, Abingdon, Oxon, OX14 3DB, UK or e-mail Publications.Officer@euro-fusion.org

The contents of this preprint and all other EUROfusion Preprints, Reports and Conference Papers are available to view online free at http://www.euro-fusionscipub.org. This site has full search facilities and e-mail alert options. In the JET specific papers the diagrams contained within the PDFs on this site are hyperlinked

Isolating the Detrapping of Deuterium in Heavy Ion Damaged Tungsten via Partial Thermal Desorption

M.J. Simmonds [a], T. Schwarz-Selinger [b], J.H. Yu[a], M.J. Baldwin [a], R.P. Doerner [a], G.R. Tynan [a,c]

[a] *Center for Energy Research, UC San Diego, 9500 Gilman Dr., La Jolla, CA 92093-0417, USA*
[b] *Max-Planck-Institut für Plasmaphysik, Boltzmannstrasse 2, D-85748 Garching, Germany*
[c] *Mechanical and Aerospace Engineering, UC San Diego, 9500 Gilman Dr., La Jolla, CA 92093-0411, USA*

Partial Thermal Desorption Spectroscopy (pTDS) is used to systematically depopulate trapped deuterium (D) from heavy ion damaged tungsten (W) trap sites to isolate and resolve both their spatial location and detrapping energies. W samples were prepared identically, damaged with 5 MeV Cu ions up to a peak displacement per atom (dpa) of 0.12, and exposed to a D_2 plasma total fluence of 10^{24} D/m^2 over 1.5 hours at a temperature of 383 K. Partial TDS up to six peak temperatures, spanning 467 to 762 K, and held for 2.5 hours was carried out. Nuclear Reaction Analysis (NRA) was performed to determine the spatial profile of the D concentration remaining after pTDS. Full TDS was then performed up to 1300 K to release all remaining D.

Total D retention measured independently through NRA and TDS were in good agreement. NRA shows three zones of D populated defects: (I) the near surface at depths less than 0.1 μm, (II) the heavy ion displacement damage peaked near 1 μm, and (III) the remaining bulk with uniform intrinsic defects. The D desorption peak in zone I is removed in samples with pTDS at 597 K and higher, suggesting the plasma induced traps have a low detrapping energy. The Stopping and Range of Ions in Matter (SRIM) predicts a displacement damage profile for zone II that coincides with the D profile for the samples with pTDS at 597 K and higher. Samples prepared with pTDS below 597 K display D components in all three zones, where the D in zone II has a distinctly different profile. The complete cycle of D_2 plasma loading, to pTDS, NRA, and finally full TDS was modeled with Tritium Migration Analysis Program (TMAP) utilizing a Pseudo Trap and Temperature Partition (PTTP) scheme developed previously. Subtraction of TDS profiles for samples with consecutive pTDS temperature isolates traps that release between the two pTDS temperatures, and demonstrates at least 7 distinct release peaks. The best fit was found with detrapping energies that were near 1.0, 1.2, 1.4, 1.5, 1.7, 1.9, and 2.5 eV when modeling with instantaneous surface recombination. Our results show that heating at 762 K for 2.5 hours was sufficient to release ~99% of the D retention in heavy ion damaged W.

1. Introduction

The retention of tritium in Plasma Facing Components (PFCs) is an important issue due to both safety concerns as well as maintaining the fuel cycle in fusion devices [t_01]. The production of fusion neutrons will lead to the degradation of PFCs throughout the bulk of the material. The divertor in ITER will be made of W and a primary candidate for PFCs in future devices such as DEMO. In order to study the effects of neutron damage and tritium exposure, heavy ion damage and deuterium are used as proxies, respectively. The guidelines for the use of heavy ions to simulate neutron damage are outlined in [t_02].

Experiments conducted to study displacement damaged W utilize NRA and TDS to quantify D retention. NRA probes the near surface, depths less than ~10 μm, whereas TDS measures the released D from throughout the bulk. The NRA profile does not differentiate as to which type of defect the D is trapped within, nor if the D is mobile in between W lattice sites. Since NRA measures the sum of all D held in various traps, the type of trap cannot be inferred without simulating thermal desorption. Each release peak in TDS data is correlated to both the spatial position and detrapping energy of a particular type of defect. Furthermore, the released D measured from the surface is the result of a diffusion process coupled to multiple types of defects, each having a particular detrapping energy. The resulting TDS data may display an effective release peak, due to multiple defects with nearby detrapping energies. Experiment and theory have produced detrapping energies spanning 0.9 to 2.4 eV [t_03], with dislocations likely 0.9 to 1.3 eV, mono-vacancies 1.4 eV, and vacancy clusters 1.9 to 2.4 eV. These values are dependent on both the attempt frequency, generally assumed to be 10^{13} s^{-1}, as well as the method and value used to model surface recombination.

Previous studies [t_04] have utilized varied plasma exposure temperatures to selectively populate defects. At higher temperature, defects with lower detrapping energies can not be effectively filled with D if the release rate is large relative to the trapping rate. The increased temperature may also significantly influence the evolution of defects to be populated. For instance, mono-vacancies may be partially annealed as mobile interstitials recombine, or above ~600 K the vacancies become mobile to further anneal or agglomerate into clusters [t_05]. Thus, at high sample temperatures, the assumption of a static population of defects may no longer be valid. In addition, the increased diffusivity of D at higher temperature will likely increase retention as deeper intrinsic traps become filled. This results in the broadening of each release peak. Therefore the direct comparison of samples with various plasma exposure temperatures is not straightforward.

To better quantify the spatial location and detrapping energies associated with various defects, we devised an experiment to sequentially depopulate each defect according to detrapping energy. Whereas previous studies have assumed specific detrapping energies and spatial concentrations [t_06], this experiment aims to constrain both quantities and test if a discrete detrapping energy model accurately reflects the experimental data. All damaged samples have the same initial conditions prior to pTDS. By performing pTDS and holding the sample at a fixed elevated temperature, defects with appreciable release rates at that temperature will

depopulate. The releasing D either travels further into the material, filling traps with higher detrapping energy, or reaches the surface to escape the sample.

2. Experiment

Sample Preparation

W samples originated from a certified 99.95 wt.% powder metallurgy polycrystalline rod, 6 mm in diameter and cut into disks 1.5 mm thick. The plasma facing surface received a mirror-like finish by successive polish treatments ending with a 3 μm grit. Contaminants from polishing were removed in ultrasonic baths of acetone followed by ethanol. Next, the samples were annealed at 1173 K for 1 hour in a vacuum chamber below 10^{-4} Pa. As noted in [t_07], a broken W sample displayed elongated grains perpendicular to the surface with dimension on the order of 10 μm parallel to the surface, as viewed by a scanning electron microscope. The maximum annealing temperature is well below the recrystallization temperature, leaving an intrinsic level of various defects throughout the bulk of the sample.

Heavy Ion Damage

The previously prepared W samples were irradiated with 5.0 MeV Cu^{2+} at the TOF beamline of the tandem accelerator laboratory at Max-Planck-Institut für Plasmaphysik in Garching (IPP) while under a low vacuum of 10^{-6} Pa and held near room temperature. Details of the setup can be found in [t_08]. The beam with a full width at half maximum of 2 mm was rastered over the samples to achieve lateral homogeneity. The implanted Cu dose was 1.215×10^{18} ions/m^2 with an average flux of 2.4×10^{15} ions/m^2/s, which maintained an impurity level below the intrinsic Cu level [t_10]. In accordance with Stoller et al. [t_09], the “Quick" Kinchin-Pease option and a displacement damage threshold of 90 eV were used to calculate the displacement profile in SRIM shown in fig. 1. According to the simulation, on average each energetic Cu ion is estimated to produce a collision cascade with over 5,600 W lattice displacements.

D_2 Plasma Exposure

One undamaged sample, as well as the identically prepared Cu ion irradiated samples, were exposed to D_2 plasma with a neutral pressure of 0.7 Pa in the PISCES-E device, a plasma etcher with a 13.56 MHz RF source [t_11]. The sample holder was negatively biased to achieve an ion impact energy of 110 eV and air cooled to maintain a constant temperature of 383 K as measured by a thermocouple in contact with the rear of the sample. An RF compensated Langmuir probe inferred a flux of 1.8×10^{20} ions/m^2/s uniformly across the surface of the sample holder as detailed in [t_12]. Each sample received a total fluence of 10^{24} D/m^2 after ~1.5 hours.

Partial TDS

Samples were kept at room temperature for 25 days before being subjected to pTDS. Samples were mounted on the tip of a thermocouple within a vacuum below 10^{-6} Pa. Parabolic mirrors focused the heat from infrared lamps on the sample surface. A programmable controller

was set to heat the samples at a constant rate of 0.5 K/s before plateauing for 2.5 hours at a particular peak temperature. That is, instead of completely desorbing the sample as in a typical TDS run by reaching a peak temperature near 1300 K, temperatures well below that were chosen to selectively depopulate various traps. In what follows, the label for each pTDS sample refers to this peak and plateau temperature (e.g. “pTDS at 467 K”). It should be noted that two control samples were not thermally desorbed at this stage, one without pTDS labeled “No pTDS” and one without heavy ion damage, "No Cu".

NRA

NRA was performed at IPP Garching 20 days after pTDS. The $D(^3He,p)^4He$ nuclear reaction measured the depth profiles of D concentration as prescribed by Mayer with a detector positioned at a scattering angle of 135° [t_13]. A ^3He ion beam was used to probe the first ~6 μm of D implanted in W with decreasing energies of 3.5, 2.5, 2.0, 1.65, 1.5, 1.3, 1.1, 0.8, and 0.6 MeV. Both the energy spectra of the resultant protons and alphas were captured in solid state detectors to determine the depth distribution of the retained D as described in [t_14]. Both SimNRA and NRADC were employed to determine the most probable D concentration as a function of depth [t_15, t_16].

Full TDS

A further 18 days elapsed between NRA and a full TDS run. As described in the pTDS section, all samples were heated with a constant 0.5 K/s ramp rate up to a peak temperature above 1300 K to ensure full desorption of D. The partial pressures of H_2, HD, and D_2 were measured with a quadrupole mass spectrometer (QMS). The thermally desorbed particle flux was calculated by converting the QMS measured partial pressure via a calibrated D_2 leak. The total D flux was calculated as described in further detail by Yu [t_17], as the sum of the HD and twice the D_2 flux. Note that the HD flux was calibrated to the D_2 leak, without any further correction for ionization efficiency. Since the detection efficiency is expected to increase for ions of lighter mass this procedure leads to a small overestimation of the total D flux. However, as HD contributed only to an average of 28% to the total D flux this is of minor importance. As described previously [t_18], variable ambient laboratory humidity, temperature, and length of vacuum break influence the water content adsorbed to the TDS chamber walls. This leads to a significant H_2 background signal that was scaled to and subtracted from the raw HD and D_2 signals.

3. Results

After pTDS and prior to full TDS, the spatial profile of D concentration was measured with NRA. In fig. 1, the experimental data displays a monotonic decrease in D concentration as the pTDS temperature is increased. The NRA profiles have distinct spatial zones, labeled I-III respectively: the near surface (~ 0.1 μm), the Cu damage region (~1 μm), and the bulk of the sample’s depth. Within zone I, the control sample without damage (solid black) displays a peak D concentration near 1.5 at. % that decays exponentially with a characteristic length of 60 nm. The intrinsic defects left after sample preparation annealing (below the recrystallization

temperature) are assumed constant throughout the bulk, zone III. For Cu damaged samples, the dominant contribution to total D retention is seen in zone II. The D concentrations for pTDS temperatures of 525 K and higher largely coincide with the SRIM predicted damage profile (dot-dashed orange). The "No pTDS" and the 467 K pTDS samples have profiles that are more heavily weighted closer to the surface. The measurable D level near 2 μm suggests the D diffusion front reached beyond the SRIM profile.

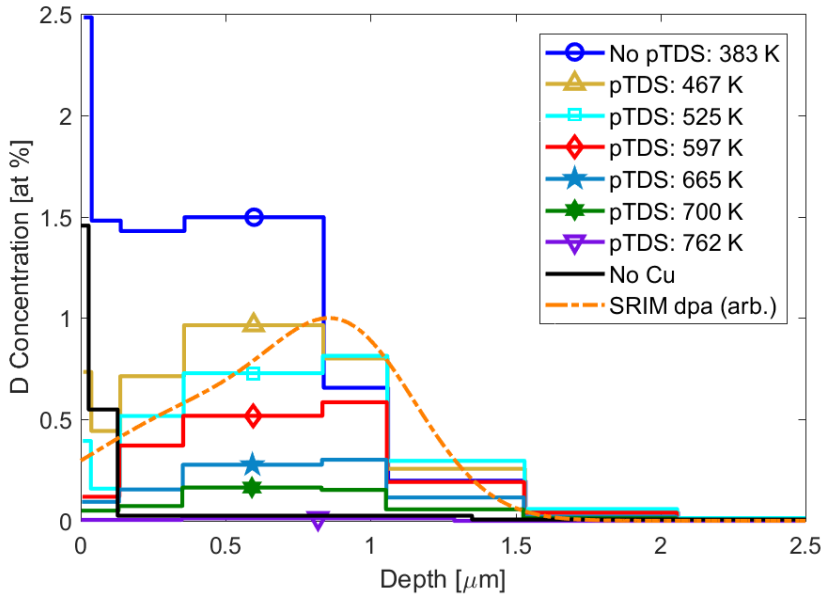

Fig. 1. The D concentration measured through NRA decreases with increasing pTDS temperature. The SRIM predicted trap profile (dot-dashed orange) for 5 MeV Cu^{2+} displays a peak near ~0.9 μm and shown here scaled to 1. Note that the experimental dose resulted in a calculated peak dpa of 0.12.

In fig. 2, the surface flux of D released from various W samples during pTDS and full TDS are shown as dashed and solid lines respectively. The experimental TDS profiles display the sequential removal of D from traps with increasing pTDS temperature. Samples heated during pTDS have a sharp drop at each plateau temperature. Not shown here, D flux plotted against time instead of temperature displays an exponential decay during the pTDS plateau. The first and weakest D filled traps are highly sensitive to surface conditions and storage time in between D implantation and TDS [t_19, t_20]. Whereas the pTDS samples were thermally desorbed after ~1 month, the control samples waited ~2 months. The extra storage time likely lead to the "No pTDS" control (dark blue) having the lowest first peak of the Cu damaged samples. The "No pTDS" control sample shows a significant increase in D as compared to the 'No Cu" control sample (black) for all temperatures below 1000 K. The initial release of the "No pTDS" control sample begins near the sample temperature during plasma exposure, 383 K. Note that the plateau pTDS temperature is at least 40 K lower than the leading edge of the initial

release temperature during full TDS. For example, the sample with pTDS plateau at 467 K (dashed gold) begins to appreciably release above 510 K (solid gold) for full TDS.

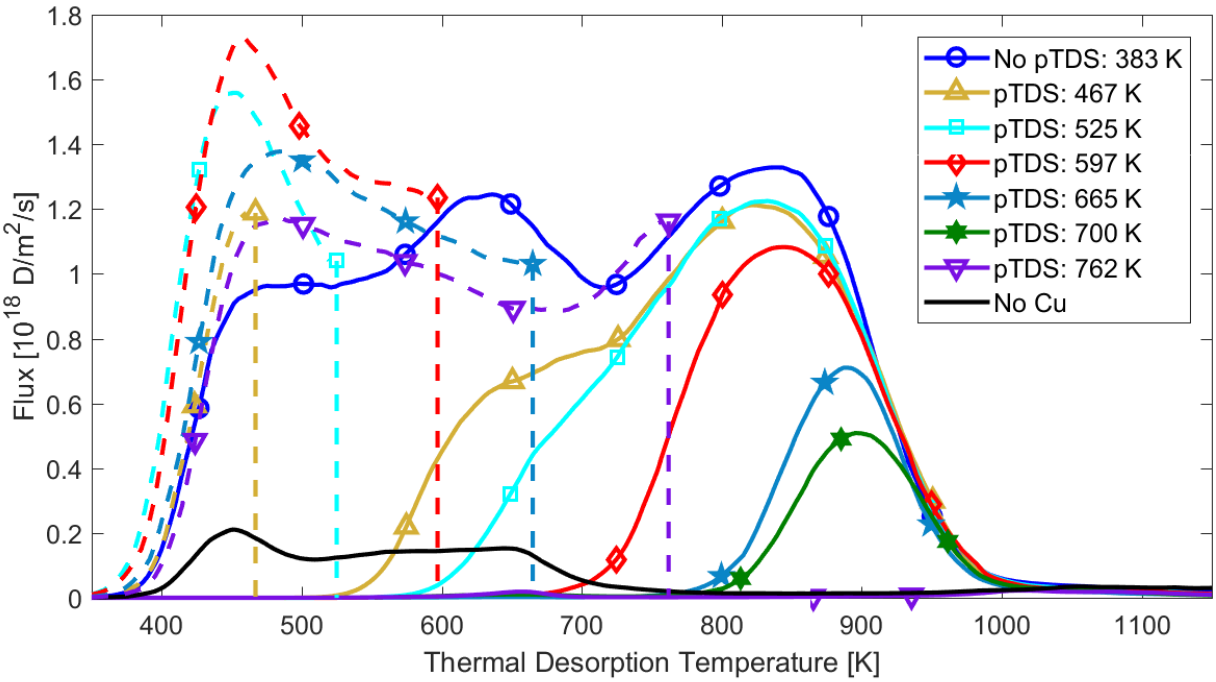

Fig. 2. The D surface flux during pTDS (dashed) and the full TDS (solid) are plotted with respect to a 0.5 K/s linear heating ramp. Once pTDS samples reached a specific peak temperature, the flux during the 2.5 hr plateau decays exponentially in time and approaches zero at this temperature.

Together, the NRA and TDS data can be used to quantify the location and concentration of D residing in each trap. In fig. 1, the NRA profiles for each of the control samples, "No Cu" and "No pTDS", have a high D concentration located in the very near surface, zone I. The first zone diminishes with increasing pTDS temperature and nearly disappears for the sample held at 597 K shown in red. Furthermore, the "No Cu" (black) and 597 K (red) samples in fig. 2 display a crossing near 700 K. The majority of the "No Cu" sample is depleted from the near surface whereas the 597 K pTDS sample is only beginning to release. Hence, plasma induced traps of zone I have relatively low detrapping energies.

Fig. 3 shows the total D retention measured during pTDS, NRA, and TDS with respect to the pTDS plateau temperature. The damaged control sample is plotted at 383 K on the x-axis and has the largest deviation between NRA and TDS measured retention, while the pTDS samples are in excellent agreement. There are a few possible reasons for the damaged control sample deviation. Though both the p and He reactants were used for NRA, this sample has the largest near surface contribution that may not be well enough resolved. Lastly, while NRA measures up to the deepest probing energy used, TDS measures the release of D throughout the bulk. With 1.5 hours of D exposure at 383 K, the D diffusion front likely exceeded the peak NRA depth of 5.5

μm. The samples heated during pTDS may have effectively released the D held in these relatively weak traps. The sum of the pTDS and TDS has a standard deviation of 1.2×10^{20} D/m^2, displaying the relative consistency of the implanted and trapped D.

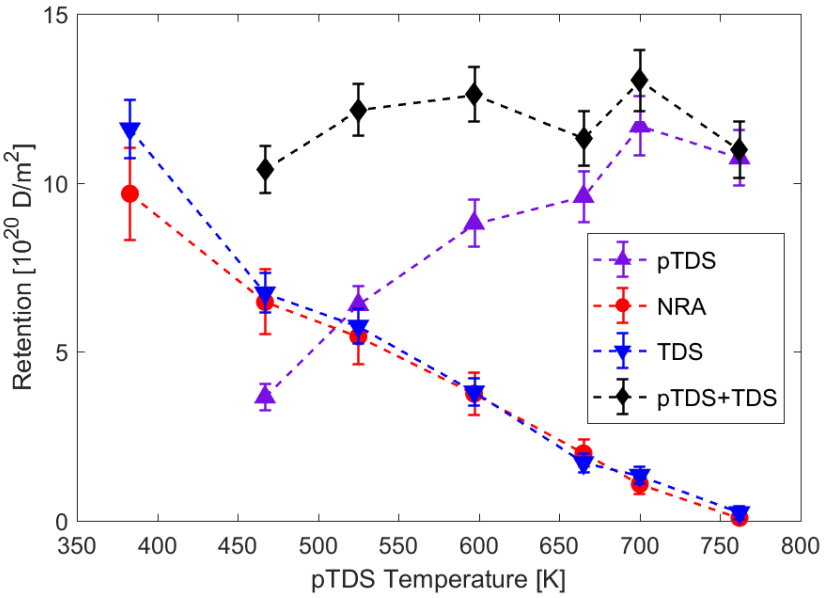

Fig. 3. The sum total D retention measured in the first 5.5 μm through NRA and the bulk through TDS. Plotted at the plasma exposure temperature of 383 K, the "No pTDS" sample shows the largest deviation from NRA. The sum of D retained measured from pTDS and TDS is consistent. Dashed lines are only to guide the eye.

4. Isolating Detrapping Energies

The simulation of the pTDS, NRA, and full TDS stages are well constrained by both the identical initial conditions and the controlled depopulation of each trap. Here we assume each trap concentration and spatial profile as well as the filling thereof during D implantation are the same for all samples. In what follows, we exploit the selective depopulation of traps with lower detrapping energies and isolated the escaped D. That is, for a given data set, we subtract the next highest pTDS temperature data set (i.e. consecutive pTDS temperatures).

NRA Subtraction

Fig. 4 and 5 display the difference between consecutive NRA D concentration profiles, ΔC, where the samples are labeled by pTDS temperature. The differences for the higher temperature pTDS samples are well fit by the SRIM predicted dpa profile (dot-dashed orange) in fig. 4. In fig. 5 an exponential with a characteristic decay length of 63 nm (dot-dashed grey) above an intrinsic concentration is shown to fit the profile for the "No Cu" sample (black). In the legend,

the "No pTDS" sample is labeled 383 K, the plasma exposure temperature. To further isolate the heavy ion damage and remove the plasma induced damage, both the 467 K and "No Cu" profiles are subtracted from the "No pTDS" profile. An empirical fit to this difference is shown as the sum of two gaussians (dot-dashed magenta) since the profile appears to have two distinct features. While fig. 4 suggests that the higher detrapping energy defects such as vacancy clusters are correlated with the SRIM predicted damage profile, fig. 5 shows the lower energy defects have a distinctly shallower profile.

Note that SRIM is a kinetic monte-carlo code that does not simulate the accumulation or agglomeration of defects and has no memory [t_21]. Each simulated energetic ion interacts with an undisturbed amorphous target that does not retain the induced damage from previous ions. The formation of defect structures such as loops or clusters is not accounted for as only displacements are counted when collisions impart enough energy to a lattice atom (i.e. above the displacement threshold). Qualitatively, SRIM predicts that the density of collision cascades increases as the heavy ion projectile loses energy to recoils and the highest density occurs at the peak dpa depth. Closer to the surface, the initially highly energetic heavy ions impart less energy to lattice atoms and are more likely to eject a single atom. The result is likely a segregation of defects, with more mono-vacancies produced towards the surface and vacancy clusters further from the surface.

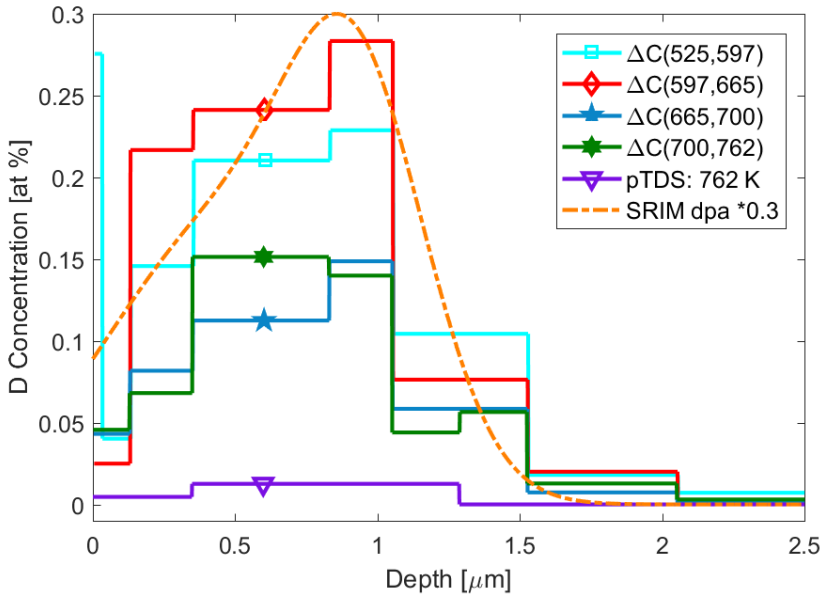

Fig. 4. The difference in D concentration between consecutive pTDS samples are shown as solid lines. The damage profile of zone II is further defined and fit well by the SRIM dpa profile scaled to 0.3 for ease of comparison (dot-dashed orange).

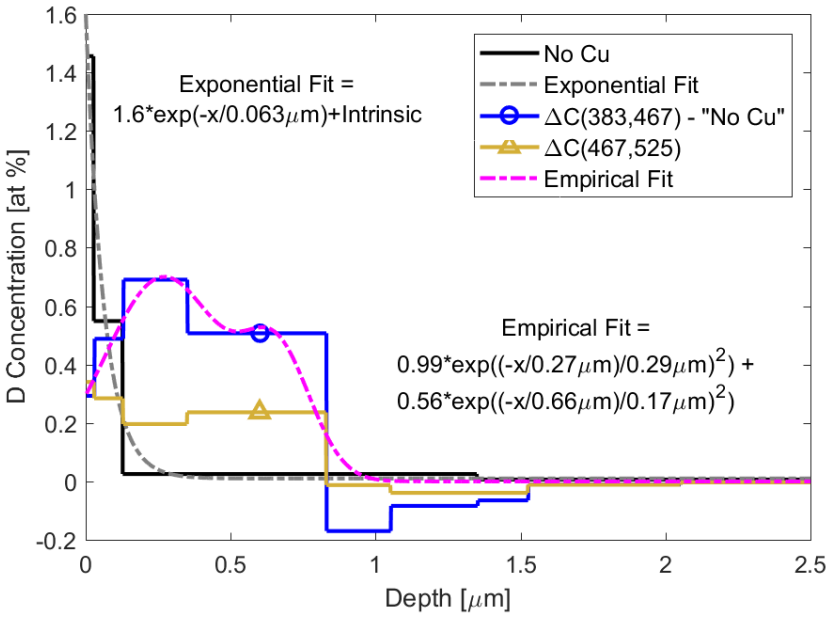

Fig. 5. The difference in D concentration between consecutive pTDS samples as well as the "No Cu" are shown as solid lines. An exponential decay (dot-dashed grey) is fit to the "No Cu" sample, defining zone I. The “No pTDS” (labeled 383 K) subtracting both the 467 K pTDS and "No Cu" is shown in blue. An empirical fit (dot-dashed magenta) to this D profile is significantly shallower than the SRIM profile.

TDS Subtraction

Similarly, the differences between the full TDS data for consecutive pTDS temperatures are shown in fig. 6. Utilizing the subtracted TDS profiles, we can infer the minimum number of distinct traps in damaged W. The first difference (dark blue) is too broad to be due to a single trap but may have at least two detrapping energies. The separation and width of each additional difference suggest at least four more individual detrapping energies. Note that the overlapping initial release of the last two deltas (turquoise and green) is likely due to the same detrapping energy. Lastly, the highest pTDS temperature at 762 K (purple) must have a unique detrapping energy of its own as evidenced by the corresponding NRA profile in fig. 4. Thus, there are at least 7 unique detrapping energies needed to model this data set with a plasma exposure temperature of 383 K.

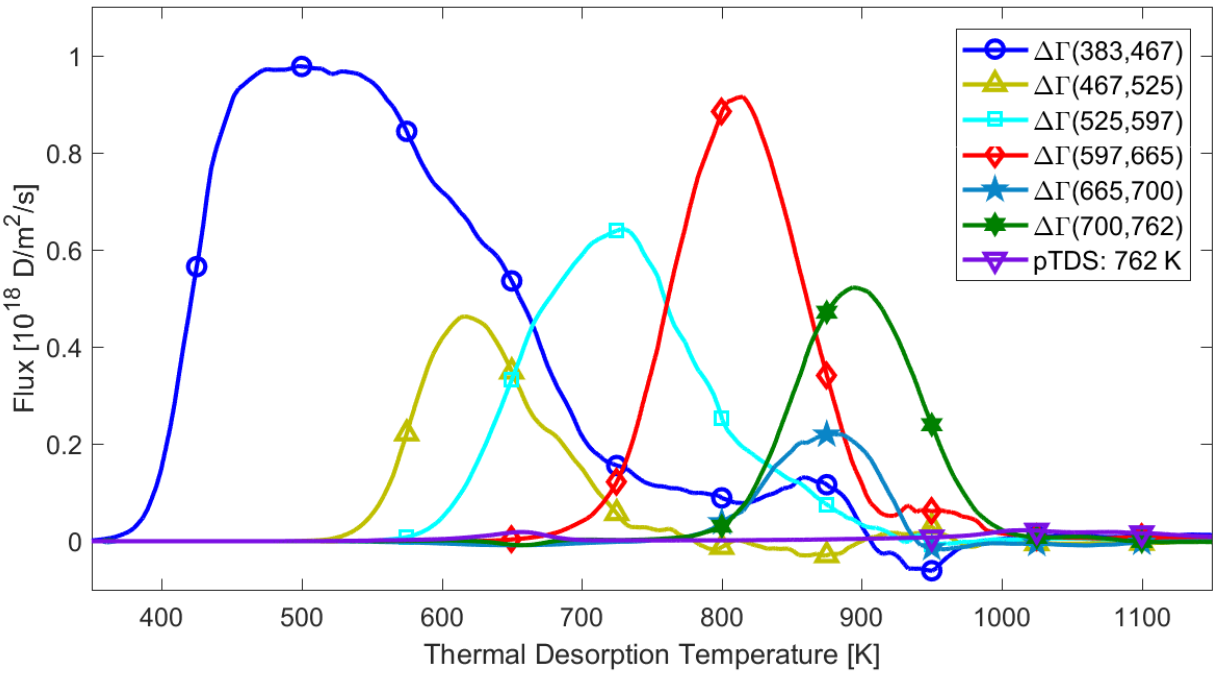

Fig. 6. The difference in D flux during full TDS, ΔΓ, for each consecutive pTDS sample pair are shown. The first dark blue line displays a broader primary peak than the other differences. Each of the remaining differences can be modeled with a single detrapping energy. All of the differences, except for the green line, begin to escape the sample at a unique temperature.

5. Simulation with PTTP

In order to utilize the well validated and verified reaction-diffusion code TMAP7 [t_22, t_23, t_24], and model more than three traps at a time, we employed a Pseudo Trap and Temperature Partitioning (PTTP) scheme outlined in [t_18]. In brief, for a particular temperature range this scheme utilizes a pseudo trap that accounts for multiple traps that do not appreciably release but may trap mobile D from solute. Applied to TMAP7, only three traps are modeled at a time, the two traps with the lowest detrapping energies and a pseudo trap, modeling all traps with higher detrapping energies.

Prior to modeling the D implantation phase, the initial conditions are defined by the sample preparation and heavy ion damage that create a trap profile. We assume the profile is composed of multiple types of defects (e.g. at least 7 for this data set) and does not evolve during the implantation or TDS phases. Each defect is differentiable by a detrapping energy and has a particular profile for three specific spatial zones as seen in fig. 1. Heavy ion damage and intrinsic defects leftover after preparation annealing act as the initial trap concentrations for zone II and III respectively. Here we also assume the plasma induced trap profile as an initial condition since the time required to induce these traps is relatively short, a few seconds, compared to the total

exposure time of over an hour. As noted earlier, only low pTDS temperatures yield a peak in D for zone I, this component is not applicable to the high energy traps (4-7). Note that the traps are ordered according to increasing detrapping energy. We also differentiate the particular trap profile in zone II for low and high energy traps as seen in fig. 4 and 5. Traps 1-3 are modeled with the empirically fit profile shown in fig. 5, whereas traps 4-7 are modeled with the SRIM predicted profile. Note that the SRIM and empirical profiles are scaled to unity (i.e. a peak value of one). The peak concentrations for each trap in each zone and the detrapping energies are the free parameters we seek to fit to the experimental NRA and TDS data. Note that the sample preparation and D implantation phase are assumed identical for all samples in this data set, thus we need only model this part of the experiment once for a given set of free parameters.

Fitting Results

All the usual reaction-diffusion parameters as outlined in [t_18, t_25] were used (e.g. mass corrected Fraunfelder diffusion coefficient). During the D exposure phase, the implanted flux was simulated as a Gaussian with mean depth taken to be ~4 nm [t_26] and 2 nm standard deviation. In the full TDS phase of the simulation, the leading edge of the surface flux began at a significantly lower temperature than the experimental TDS data. As noted previously and seen in fig. 2, the pTDS temperature does not exactly coincide with the appreciable release. In order to bring the simulated release closer to the experimental value, the Anderl recombination coefficient was replaced with instantaneous surface recombination. Neglecting surface recombination allowed the use of Eckstein's reflection coefficient value, ~0.65.

The full cycle was simulated and all free parameters were optimized utilizing the technique of simulated annealing [t_27]. During the simulated annealing, the free parameters were constrained according to the differences in consecutive TDS and NRA data previously outlined. The simulation of a particular set of trap parameters results in unique NRA and TDS profiles. Both the experimental and simulation data were interpolated to a finely spaced grid to directly compare the "goodness of fit." The Normalized Root Mean Square Error (NRMSE) as well as the residual, the absolute difference between experiment and simulation, were the metrics used to determine the optimal fit. In addition, the resulting NRMSE and residuals were weighted with respect to their total D retention and added together to determine a single fit metric. For instance, the "No pTDS" sample had the highest D retention and had the largest weighting as the highest temperature pTDS at 762 K contributed the least weight when determining the best fit parameters.

The number of traps used to simulate the experiment was varied up to 8. As outlined in the section on TDS subtraction, the best fit was found to need at least 7 traps with detrapping energies near 1.0, 1.2, 1.4, 1.5, 1.7, 1.9, and 2.5 eV. Using 8 traps, nearly the same energies were found and one additional energy of 2.3 eV produced nearly the same fit metric. We note that the results shown are based on the PTTP scheme that assumes a minimal separation in detrapping energies. For instance, a difference below 0.1 eV for consecutive detrapping energies leads to a

significant error as outlined in [t_18]. Table 1 is a summary of the resulting free parameters found to give the best fit with the least number of traps, in this case 7.

Table 1. Summary of the best fit parameters for each trap. The peak concentrations in each zone and the detrapping energies modeled using the PTTP scheme.

Trap No.	Zone I [at. %]	Zone II [10^{-1} at. %]	Zone II Profile Shape	Zone III [10^{-3} at. %]	Energy [eV]
1	0.2	3.0	Empirical	1.3	1.00
2	2.1	3.0	Empirical	1.3	1.19
3	0.8	5.2	Empirical	0.5	1.37
4	N/A	2.1	SRIM	0.9	1.51
5	N/A	5.0	SRIM	0.6	1.73
6	N/A	3.0	SRIM	0.4	1.92
7	N/A	0.05	SRIM	~ 0.0	2.50

The simulated NRA and TDS profiles (dashed lines) are compared to the experimental data (solid lines) in fig. 8 and 9 respectively. The simulated NRA and TDS produced reasonable fits with average NRMSE values of ~0.7 for both. A possible reason for the discrepancy may be due to using only 7 detrapping energies. For instance, what appears as a single peak in fig. 9 can be made of several nearby detrapping energies. If three detrapping energies made the peak near 620 K, the lowest energy may be completely released, the middle partially, and the highest remained filled for a pTDS at 467 K (gold). Several more experimental data points would be needed to discern this discrepancy.

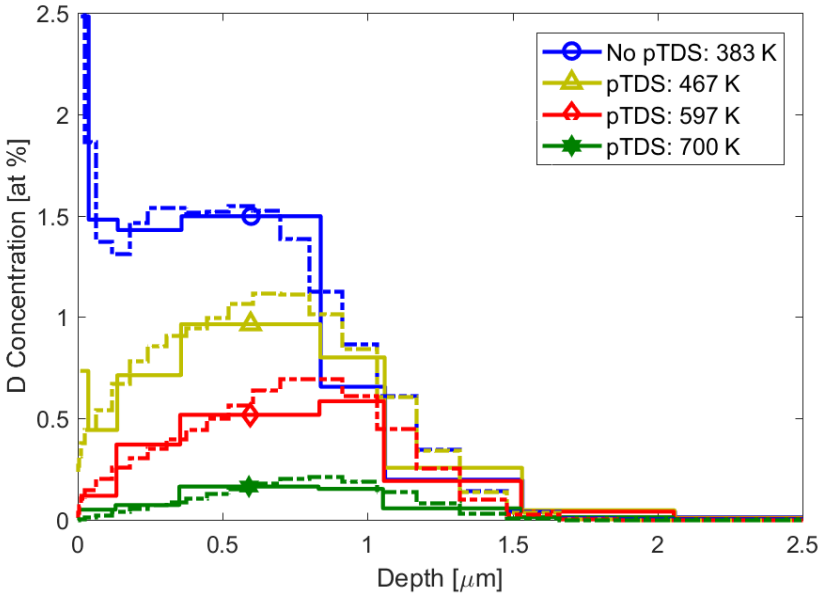

Fig. 8. The comparison of the NRA data (solid) and the simulation result (dashed) using the optimized fit parameters, summarized in Table 1. For clarity, only 4 samples are shown.

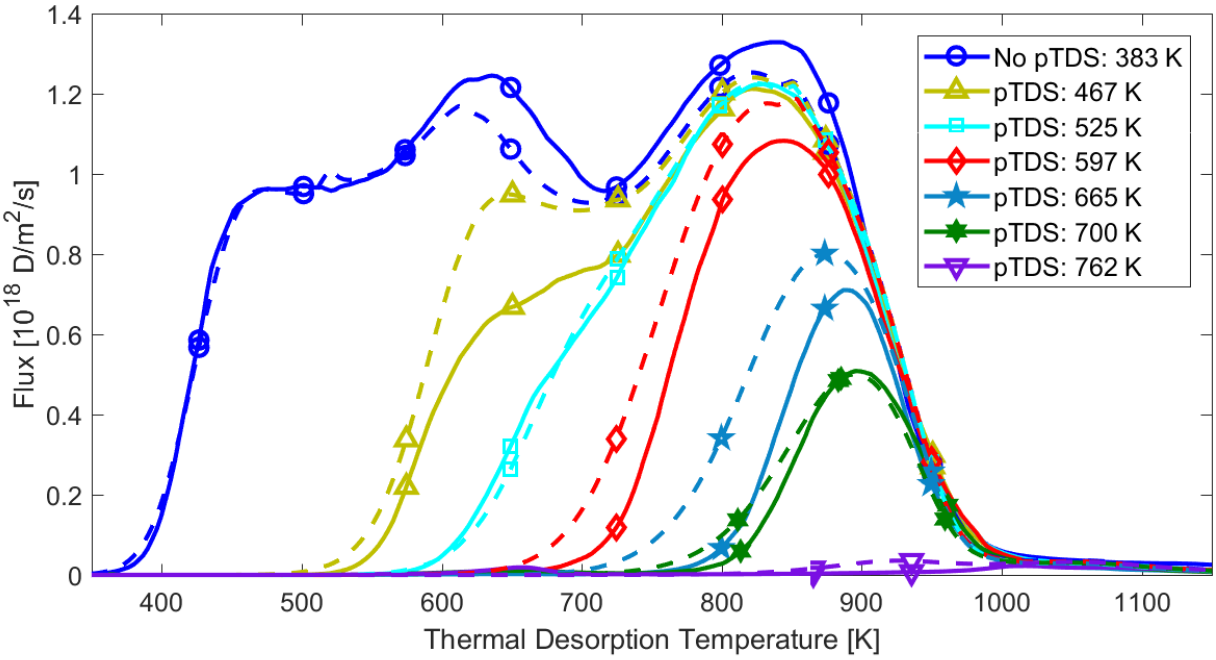

Fig. 9. The comparison of the TDS data (solid) and the simulation result (dashed) using the optimized fit parameters, summarized in Table 1.

6. Discussion

The detrapping energies found reflect similar values observed in previous studies [t_06]. Ogorodnikova speculates the type of defect likely associated with each detrapping energy [t_13]. Specifically, the two lowest energies of 1.0 and 1.2 eV are likely due to grain boundaries. Trap 3 at 1.4 eV is due to mono-vacancies as seen by studies that use light ion damage to eject a single W from a lattice site [t_28]. For traps 4 through 7 with detrapping energies of 1.5 to 2.5 eV, the types of defects are likely related to vacancy complexes, voids, and dislocations.

Recent work done with x-ray spectroscopy [t_29] has quantified the number of defects due to dislocation loops. For a single crystalline W sample damaged at 5 MeV up to 0.2 dpa, the vacancy type loops concentration was near 0.1 atomic percent. This experiment did not resolve vacancy defects with radii below 5 Å, thus the quoted vacancy concentration is for complexes and does not include mono, di, or even tri-vacancies. Traps 4-6 are related to vacancy complexes and have atomic concentrations of the same order of magnitude. The x-ray data also yields the size distribution, where the largest complexes are nearly two orders of magnitude lower in

concentration than the smallest (5 Å) loop. Having the largest detrapping energy, trap 7 is likely due to a large vacancy complex and has a concentration nearly two order of magnitude lower than traps 4-6.

Shown in fig. 5, the segregation of defects induced during ion damage is an important factor to consider when comparing to neutron damage. While the neutron only interacts with the nuclei of lattice W, the electronic stopping loss of heavy ions produces a distinctly unique profile for various defects. The difference in defect profiles for vacancy complexes is likely below the resolution of NRA, but we have shown evidence for a significant deviation between the high and low detrapping energies. The defects with higher detrapping energies (traps 4-7) correlate to the SRIM predicted Bragg peak while defects with low detrapping energies (e.g. mono-vacancies) are shallower. The neutron damage profile in PFMs must be spatially uniform since there is no electronic stopping loss to create a Bragg peak.

7. Summary

Trapped D in Cu ion damaged W was sequentially depopulated with increasing temperature to determine the spatial profile and detrapping energies. The total D retention measured through pTDS, NRA, and TDS are shown to be in excellent agreement as well as demonstrating the repeatability of sample preparation. Comparing the NRA data from the control sample, without pTDS, and the lowest pTDS temperatures demonstrates that all of the plasma induced defects in the near surface were depopulated by holding the sample at 597 K. In addition, the majority of retained D is depopulated by a pTDS temperature of 762 K. For pTDS peak temperatures between 525 and 762 K, the D profiles measured via NRA are similar to the displacement damage profile predicted by SRIM. The full cycle of D_2 plasma loading, to pTDS, and finally a full TDS cycle was modeled with TMAP7 utilizing a Pseudo Trap and Temperature Partition (PTTP) scheme. Detrapping energies near 1.0, 1.2, 1.4, 1.5, 1.7, 1.9, and 2.5 eV were found to fit the experimental data.

8. Acknowledgements

This work was supported by U.S. Department of Energy under DE-FG02-07ER54912 and DE-SC0001999 as well as the University of California Office of Presidential Research Fund under 12-LR-237801. Part of this work has been carried out within the framework of the EUROfusion Consortium within the work project PFC and has received funding from the Euratom research and training programme 2014-2018 under grant agreement No 633053. The views and opinions expressed herein do not necessarily reflect those of the European Commission.

9. References

[t_01] V. Philipps, Tungsten as material for plasma-facing components in fusion devices, Journal of Nuclear Materials, Volume 415, Issue 1, 2011, Pages S2-S9.

[t_02] A. E521, Standard Practice for Neutron Radiation Damage Simulation by Charged-Particle Irradiation (1996). Reapproved 2009

[t_03] Ogorodnikova paper with detrapping energies modeled

[t_04] Ogorodnikova paper with varied temperature of D exposure

[t_05] F. Ferroni, X. Yi, K. Arakawa, S. P. Fitzgerald, P. D. Edmondson, S. G. Roberts, High temperature annealing of ion irradiated tungsten, Acta Materialia 90 (2015) 380 – 393.

[t_06] Papers with assumptions about spatial distribution and detrapping energies

[t_07] M.J. Simmonds *et al*., Reduced Deuterium Retention in Simultaneously Damaged and Annealed Tungsten, J. Nuclear Mat. 494 (2017) 67-71.

[t_08] T. Schwarz-Selinger, "Deuterium Retention in MeV Self-Implanted Tungsten: Influence of Damaging Dose Rate." Nuclear Materials and Energy, March 2017. https://doi.org/10.1016/j.nme.2017.02.003.

[t_09] R. Stoller, M. Toloczko, G. Was, A. Certain, S. Dwaraknath, F. Garner, On the use of SRIM for computing radiation damage exposure, Nuclear Instruments and Methods in Physics Research Section B: Beam Interactions with Materials and Atoms 310 (2013) 75 - 80.

[t_10] J. Barton, Y. Wang, T. Dittmar, R. Doerner, G. Tynan, Deuterium retention in tungsten after heavy ion damage and hydrogen isotope exchange in PISCES, Nucl. Instrum. Methods Phys. Res. Sect. B Beam Interact. Mater. Atoms, 332 (2014), pp. 275-279

[t_11] G. R. Tynan, A. D. B. III, G. A. Campbell, R. Charatan, A. de Chambrier, G. Gibson, D. J. Hemker, K. Jones, A. Kuthi, C. Lee, T. Shoji, M. Wilcoxson, Characterization of an azimuthally symmetric helicon wave high density plasma source, Journal of Vacuum Science & Technology A 15 (1997) 2885–2892

[t_12] M.J. Baldwin, R.P. Doerner, Hydrogen isotope transport across tungsten surfaces exposed to a fusion relevant He ion fluence, Nuclear Fusion Vol. 57, 2017

[t_13] O.V. Ogorodnikova, Fundamental aspects of deuterium retention in tungsten at high flux plasma exposure, J. Appl. Phys., 118 (2015), p. 074902

[t_14] M. Mayer, E. Gauthier, K. Sugiyama, U. von Toussaint, Quantitative depth profiling of deuterium up to very large depths, Nucl. Instrum. Methods Phys. Res. Sect. B Beam Interact. Mater. Atoms, 267 (2009), pp. 506-512

[t_15] M. Mayer, SIMNRA, a simulation program for the analysis of NRA, RBS and ERDA , AIP Conf. Proc., 475 (1999), pp. 541-544

[t_16] K. Schmid, U. von Toussaint, Statistically sound evaluation of trace element depth profiles by ion beam analysis, Nucl. Instrum. Methods Phys. Res. Sect. B Beam Interact. Mater. Atoms, 281 (2012), pp. 64-71

[t_17] J.H. Yu, M. Simmonds, M.J. Baldwin, R.P. Doerner, Deuterium desorption from tungsten using laser heating, Nuclear Materials and Energy, Volume 12, 2017, Pages 749-754, ISSN 2352-1791

[t_18] M.J. Simmonds, Y.Q. Wang, J.H. Yu, M.J. Baldwin, R.P. Doerner, G.R. Tynan, Expanding the capability of reaction-diffusion codes using pseudo traps and temperature partitioning: Applied to hydrogen uptake and release from tungsten, Journal of Nuclear Materials (Under Review)

[t_19] O.V Ogorodnikova, J Roth, M Mayer, Deuterium retention in tungsten in dependence of the surface conditions, In Journal of Nuclear Materials, Volumes 313–316, 2003, Pages 469-477, ISSN 0022-3115

[t_20] Jonathan’s paper has a desorption reference for outgassing as a function of storage time

[t_21] J. Ziegler, J. Biersack, U. Littmark, The stopping and range of ions in matter, Pergamon Press (1985).

[t_22] B.J. Merrill, Jones J.L. and Holland D.F. 1986 TMAP/Mod 1: tritium migration analysis program code description and user’s manual *Idaho, Inc., Idaho National Engineering Laboratory (Idaho,)* EGG-EP-7407, EG and G

[t_23] G:R. Longhurst G.R. 2008 TMAP7 user manual *Idaho National Engineering and Environment Laboratory(Idaho Falls, Idaho,)* INEEL/EXT-04-02352(Rev. 2)

[t_24] J. Ambrosek and Longhurst G.R. 2008 Verification and validation of TMAP7 Idaho National Engineering and Environment Laboratory (Idaho Falls, Idaho,) INEEL/EXT-04-01657(Rev. 2)

[t_25] M. Poon, A.A. Haasz, J.W. Davis, Modelling deuterium release during thermal desorption of D+-irradiated tungsten, In Journal of Nuclear Materials, Volume 374, Issue 3, 2008, Pages 390-402, ISSN 0022-3115

[t_26] Eckstein W 2002 Calculated sputtering, reflection and range values IPP-Report IPP 9/132 (Max-Planck-Institut für Plasmaphysik, Garching)

[t_27] Simulated Annealing reference

[t_28] M. Zibrov, S. Ryabtsev, Yu. Gasparyan, A. Pisarev, Experimental determination of the deuterium binding energy with vacancies in tungsten, Journal of Nuclear Materials, Volume 477, 2016, Pages 292-297, ISSN 0022-3115

[t_29] X-Ray paper from SLAC (Under Review)

[x_1] O.V. Ogorodnikova, S. Markelj, U. von Toussaint, Interaction of atomic and low-energy deuterium with tungsten pre-irradiated with self-ions, J. Appl. Phys. 119 (2016) 054901.

[x_2] O.V Ogorodnikova, J Roth, M Mayer, Ion-driven deuterium retention in tungsten, In Journal of Applied Physics, Volume 103, 2008, Pages 034902